Novel Reference Region Model Reveals Increased Microglial and Reduced Vascular Binding of ^{11}C-(*R*)-PK11195 in Patients with Alzheimer's Disease

Giampaolo Tomasi[1], Paul Edison[2,3], Alessandra Bertoldo[1], Federico Roncaroli[2], Poonam Singh[2], Alexander Gerhard[4], Claudio Cobelli[1], David J. Brooks[2,3], and Federico E. Turkheimer[2,3]

[1]Department of Information Engineering, University of Padova, Padova, Italy; [2]Division of Neuroscience and Mental Health, Clinical Neuroscience and Neuropathology Departments, Imperial College London, London, United Kingdom; [3]MRC Clinical Sciences Centre, Hammersmith Hospital, London, United Kingdom; and [4]Wolfson Molecular Imaging Centre, University of Manchester, Manchester, United Kingdom

^{11}C-(*R*)-PK11195 is a PET radiotracer for the quantification of peripheral benzodiazepine binding sites (PBBSs). The PBBS is a consistent marker of activated microglia, and ^{11}C-(*R*)-PK11195 has been used to image microglial activity in the diseased brain and in neoplasia. However, the PBBS is also expressed in the brain vasculature (endothelium and smooth muscles), and no evidence, to our knowledge, exists of a change in the vascular PBBS in pathologic brains or of such a change having an effect on the quantification of ^{11}C-(*R*)-PK11195 binding. To investigate this issue, we have used a modified reference-tissue model (SRTMV) that accounts for tracer vascular activity both in reference and target tissues and applied it for the estimation of binding potential (BP) in a cohort of patients with Alzheimer's disease (AD). **Methods:** A total of 10 patients with AD and 10 age-matched healthy subjects who underwent a ^{11}C-(*R*)-PK11195 scan were considered in the analysis. The time–activity curves of 11 regions of interest were extracted using the Hammersmith maximum probability atlas. BPs were first estimated using the standard simplified reference-tissue model (SRTM) with the reference tissue computed with a supervised selection algorithm. Subsequently, we applied an SRTMV that models PBBS vascular activity using an additional linear term for both target (Vb^T) and reference (Vb^R) regions accounting for vascular tracer activity (C_B), whereas C_B was extracted directly from the images. Vb^R was fixed to 5%, and R_1, k_2, BP, and Vb^T were estimated. PBBS density in the vasculature was also assessed by immunocytochemistry on a separate cohort of young and elderly controls and 3 AD postmortem brains. **Results:** The inclusion of a vascular component in the SRTM increased BPs in all subjects, but the amount of the increase was different (about 11.9% in controls and 16.8% in patients with AD). In addition, average Vb^T values derived using the SRTMV were 4.22% for controls but only 2.87% in patients with AD. Immunochemistry showed reduced PBBS expression in AD due to vascular fibrosis. **Conclusion:** The reduction of Vb^T in AD can be interpreted as a consequence of 2 independent but concurring phenomena. The vascular fibrosis in the AD brain causes the well-documented decrease of the size of lumens and the reduction of blood volume. At the same time, the fibrotic process determines the loss of vascular PBBS, particularly in smooth muscles, as here documented by immunochemistry. The inclusion of the additional vascular component in the SRTM effectively models these 2 concurrent processes and amplifies the BP in AD more than in controls because of the decrease in tracer binding to the vasculature in the disease cohort.

Key Words: PET; simplified reference region modeling; ^{11}C-(*R*)-PK11195; Alzheimer's disease; vascular fibrosis

J Nucl Med 2008; 49:1249–1256
DOI: 10.2967/jnumed.108.050583

The isoquinoline ^{11}C-(*R*)-PK11195 is a selective ligand for the peripheral benzodiazepine binding sites (PBBSs), and it is widely used for tracing activated microglia in a variety of disorders of the central nervous system (*1,2*). The PBBS is an 18-kDa protein that functions as a cholesterol transporter and is expressed mainly in mitochondria (*1*). High levels of PBBSs are expressed in the adrenal cortex, kidney, heart, and lungs (*3*), whereas the normal brain shows detectable levels only in the choroid plexus, ependyma, olfactory bulbs, endothelial cells, and smooth muscle of the tunica medium of intra- and extraparenchymal arteries (*4*).

Quantification of ^{11}C-(*R*)-PK11195 in PET studies uses the simplified reference-tissue model (SRTM) (*5*). In a recent study, we chose the appropriate reference region by using a supervised selection algorithm that, by fitting the time–activity curve of each pixel with a database of tissue kinetics (normal gray and white matter, vascular, muscle, skull, and pathologic tissue with high active microglia density), defines a reference gray matter tissue devoid of specific PBBS binding (*4*). In the course of that work, we showed significant PBBS density in the brain vasculature in smooth muscles and endothelial cells and demonstrated a characteristic slow

Received Oct. 22, 2007; revision accepted Apr. 23, 2008.
For correspondence or reprints contact: Federico E. Turkheimer, Division of Neuroscience and Mental Health, Department of Clinical Neuroscience, Cyclotron Building, Room 236, Hammersmith Hospital, DuCane Rd., London W12 0NN, U.K.
E-mail: federico.turkheimer@imperial.ac.uk

binding of ^{11}C-(*R*)-PK11195 to these sites. Furthermore, by testing a wide range of methodologies for parametric map formation, we have identified in the SRTM the optimal kinetic methodology to provide highly reproducible maps of microglial activity, if applied with a supervised reference extraction (*6*). However, none of the approaches used so far has included the vasculature tracer information in the modeling, implicitly assuming the same vascular volume both in healthy conditions and in disease.

In the normal brain, neurons, astrocytes, and vascular cells are part of integrated functional units aimed at maintaining homeostasis (*7,8*). One can therefore expect cerebrovascular dysregulation not only in cerebrovascular pathologies, such as stroke, in which the blood–brain barrier is impaired, but also in neurodegenerative conditions that may not necessarily imply blood–brain barrier disruption but cause significant changes in vascular cell protein expression (*9*). We chose Alzheimer's disease (AD) as a representative disease model to verify the effects of the introduction of a vascular component into the quantification of ^{11}C-(*R*)-PK11195 and performed histocytochemistry on AD postmortem brains to verify observations made from PET-estimated models.

MATERIALS AND METHODS

Radiochemistry

R-[*N*-methyl-^{11}C]PK11195 was synthesized by methylation of the precursor R-*N*-desmethyl-PK11195, using no-carrier-added ^{11}C-methyl iodide as the methylation reagent. No-carrier-added ^{11}C-carbon dioxide was produced using a cyclotron (PETtrace; GE Healthcare) by the ^{14}N(p,α)^{11}C reaction on nitrogen gas containing 1% oxygen, using protons (incident energy, 16 MeV) and a beam current of 55 μA. This was bubbled into a solution containing 200 μL of 0.1 M $LiAlH_4$. After elimination of the solvent, 200 μL of 57% hydrogen iodide was added to the reactor and heated to 160°C. [^{11}C]CH_3I was distilled under a stream of nitrogen into a reaction vessel containing 1 mg of precursor, 1.5 mg of dry potassium hydroxide, and 200 μL of dimethyl sulfoxide. The reaction vessel was then sealed and heated to 90°C for 90 s. The reaction mixture was injected onto a reverse-phase high-performance liquid chromatography column and eluted with a mixture of ethanol and water (70:30, v/v) at 3 mL/min. The final radioactive product was formulated for intravenous administration by evaporating the collected fraction to dryness, dissolving the radioactive residue in isotonic saline containing ethanol (5%, v/v), and filtering using sterile technique.

The radiochemical yield of the filtered product was typically 2–4 GBq (74–148 mCi) at the end of synthesis. Each product was analyzed by reverse-phase high-performance liquid chromatography and found to have greater than 99% radiochemical purity, greater than 99% chemical purity, and a specific radioactivity of 133–300 GBq/μmol (3.4–8.1 Ci/μmol) at the end of synthesis.

Imaging

All ^{11}C-(*R*)-PK11195 studies were performed on a 3-dimensional PET camera (ECAT EXACT; CTI/Siemens) with a 23.4-cm axial field of view, 95 transaxial planes, and a spatial resolution of 4.8-mm (transaxial) and 5.6-mm (axial) full width at half maximum (*10*). Three-dimensional sinograms of emission data were then acquired over 60 min as 18 time frames (1 × 30 s background frame and 1 × 15, 1 × 5, 1 × 10, 1 × 30, 4 × 60, 7 × 300, and 2 × 600 s frames). Volumetric T1-weighted MR images were obtained on a 1.0-T scanner (HPQ; Picker) at the Robert Steiner MR Unit, Hammersmith Hospital. Further details on the procedure used can be found in Turkheimer et al. (*4*). The dataset used consisted of 10 healthy subjects and 10 age-matched patients with AD. Average injected activity was 286 MBq for each scan. The MRI of each patient was coregistered to its PET summed image using statistical parametric mapping (SPM5; Functional Imaging Laboratory, Wellcome Department of Imaging Neuroscience, University College London). The coregistered MR images were then normalized to the MNI/ICBM152 (MNI is Montreal Neurological Institute; ICBM is International Consortium for Brain Mapping) space, and the parameters obtained from the normalization process for each subject were used to obtain a normalized PET dynamic image. Region-of-interest (ROI) time–activity curve extraction was performed on the normalized PET images using the Hammersmith maximum probability atlas (*11*). The 11 ROIs were cerebellum, lateral occipital lobe, anterior cingulate gyrus, posterior cingulate gyrus, frontal lobe middle frontal gyrus, posterior temporal lobe, parietal lobe, thalamus, superior parietal gyrus, occipital lobe lingual gyrus, and occipital lobe cuneus.

Analysis of PET Data

A reference-region modeling approach was used to quantify tracer data. For each subject, the extraction of the reference-region time–activity curve was performed on the original PET image using the supervised algorithm presented in Turkheimer et al. (*4*). The modified version of SRTM that we used, which takes into account the tracer activity in the vasculature, was originally proposed in Gunn et al. (*12*) and subsequently developed and applied in Bertoldo et al. (*13*). The equations describing the modified reference-tissue model (SRTMV) can be easily obtained as follows:

$$C_T^{MEAS}(t) = (1 - Vb^T)C_T^{TRUE}(t) + Vb^T C_B(t) \qquad \text{Eq. 1}$$

$$C_R^{MEAS}(t) = (1 - Vb^R)C_R^{TRUE}(t) + Vb^R C_B(t). \qquad \text{Eq. 2}$$

$C_T(t)$ and $C_R(t)$ denote, respectively, the target and reference-region time–activity curve (the true time–activity curve or the measured one, according to the apex) (MBq/mL), $C_B(t)$ indicates vasculature tracer activity (MBq/mL), and Vb^T (unitless) and Vb^R (unitless) refer to the fraction of tracer activity in the vascular space in the target and reference region, respectively. In the present study, $C_B(t)$ was derived noninvasively from the PET images. Thus, when a tracer such as ^{11}C-(*R*)-PK11195 expresses vascular cell protein, $C_B(t)$ is supposed to indicate all the overall tracer time–activity in the vasculature (i.e., plasma, red cells, and the vascular binding to endothelium and smooth muscles, assuming negligible partial volume). Consequently, Vb is the fraction of the measured tracer activity due to the brain vasculature.

Consider now the standard SRTM model equation:

$$C_T^{TRUE}(t) = R_1 C_R^{TRUE}(t) + \left[k_2 - \frac{k_2 R_1}{1+BP}\right] C_R^{TRUE}(t) \otimes e^{-\frac{k_2}{1+BP}t}, \qquad \text{Eq. 3}$$

where BP (unitless) is the binding potential, k_2 (min^{-1}) is the efflux rate constant from the target pixel or ROI, and R_1 (unitless) is the ratio of the delivery in the tissue pixel or ROI to that of the

reference region (ratio of influx). Assuming $Vb^T = Vb^R = 0$, one gets $C^{MEAS}(t) = C^{TRUE}(t)$ for both target and reference regions from Equations 1 and 2 and, therefore, can directly use Equation 3 to estimate R_1, k_2, and BP. If the previous assumption is not made, solving Equations 1 and 2 for $C_T{}^{TRUE}(t)$ and $C_R{}^{TRUE}(t)$, respectively, and inserting the results into Equation 3 leads to:

$$C_T{}^{MEAS}(t) = Vb^T C_B(t) + \frac{1 - Vb^T}{1 - Vb^R}\left\{R_1(C_R{}^{MEAS}(t) - Vb^R C_B(t)) + \ldots\left[k_2 - \frac{k_2 R_1}{1+BP}\right](C_R{}^{MEAS}(t) - Vb^R C_B(t)) \otimes e^{-\frac{k_2}{1+BP}t}\right\}. \quad \text{Eq. 4}$$

Equation 4 expresses the known measured time–activity curve of the target region as a function of the measured reference time–activity curve and of the whole-blood time–activity curve. The parameters to be estimated are now R_1, k_2, and BP as before, plus Vb^T and Vb^R, the fraction of vascular tracer activity in the target and reference region, respectively. Both SRTM (R_1, k_2, and BP) and SRTMV (R_1, k_2, BP, Vb^T, and Vb^R) parameters are a priori uniquely identifiable (*14*). However, in the SRTMV, because Vb^R has a fixed (unknown) value independent of the target regions, we fixed it at the conventional value of 0.05, which leads to more stable and reliable estimates of the other parameters, especially when working at pixel level (*13*). We also investigated the changes of the estimated target blood volumes for different values of Vb^R (0.06, 0.07, and 0.08). We chose a grid of values for Vb^R according to Kropholler et al. (*15*), who estimated via arterial blood sampling a Vb of 7.1% for ^{11}C-(*R*)-PK11195. The effect of fixing Vb^R instead of estimating it was also tested, as the assumption of a reasonably constant Vb^R across different subjects may not be accurate. We first estimated a Vb^R computed via nonlinear least squares (for a total of 5 parameters for each ROI), then we fixed it for each subject to the mean value across the 11 ROIs, and then we reestimated each parameter with Vb^R fixed but to a value that was subject-dependent.

The estimation of model parameters can be obtained through nonlinear least-squares estimation. However, to reduce computational time, a basis-function approach (*16*) can be used alternatively. For each fixed value of a grid of plausible values for the parameter $\vartheta = \frac{k_2}{1+BP}$, one can solve the resulting problem that is linear in the parameter vector $p = (p_1, p_2) = (R_1, k_2 - \frac{k_2 R_1}{1+BP})$ for SRTM and $p = (p_1, p_2, p_3) = (Vb^T, [1-Vb^T]R_1, [1-Vb^T][k_2 - \frac{k_2 R_1}{1+BP}])$ for SRTMV and in the end retain the value of $\vartheta_{OPTIMUM}$, which gives rise to the smallest weighted sum of residuals together with the parameter vector $p_{OPTIMUM}$ (the output of the corresponding linear estimation). By suitably combining $\vartheta_{OPTIMUM}$ and the elements of $p_{OPTIMUM}$, one can obtain R_1, k_2, and BP for SRTM and R_1, k_2, BP, and Vb^T for SRTMV. For both SRTM and SRTMV, the inverse of frame durations were used as weights for the parameter estimation.

Whole Vasculature Time–Activity Curve Extraction

For most patients, no invasive measurement of the arterial tracer concentration was available. Even if the measurement was available, however, the use of the measured $C_B(t)$ in SRTMV would violate the basic idea underlying the reference-tissue model, which was developed to avoid such invasive and sometimes unfeasible measurements. To estimate the whole $C_B(t)$ directly from the PET image noninvasively, we used the following algorithm. In the whole brain we selected the 10 pixels with the maximum value in the first 5 frames, which were the ones in which the blood tracer concentration has its peak. The mean of the selected time–activity curves of the pixels was used as $C_B(t)$. This simple procedure is significantly faster than any approach based on cluster or on manual selection of the vascular components and is user-independent. The choice of 10 pixels was based on a compromise between the need to obtain a sharp peak for $C_B(t)$, which would require use of the smallest possible number of pixels, and the need to obtain reliable and regular curves. We also computed kinetic parameters for each subject, estimating $C_B(t)$ using the 5 and 20 pixels with the highest values in the first frames to test the robustness of the algorithm with the number of pixels used for the estimation of $C_B(t)$.

Immunohistochemical Data

We examined 9 brains retrieved from the files of the Corsellis Collection. Three were normal brains of young subjects (aged 30, 30, and 35 y); 3 were normal brains of individuals aged 80 y, with no history of neurodegenerative disease; and 3 were brains of individuals with AD (aged 60, 66, and 69 y). A full postmortem examination was performed on all cases. The 6 healthy individuals died of acute vascular accident and had no evidence of infectious or neoplastic disease. Brains were fixed in 4% buffered formalin for a minimum of 4 wk, and samples taken during dissection were embedded in wax. Neuropathologic work-up was performed on the hematoxylin-eosin–stained section. Diagnosis of AD was confirmed by staining the frontal lobe and hippocampus with antibodies directed against phosphorylated τ (AT8, dilution 1:800) (NBS Biochemical) and amyloid-β peptide (monoclonal 6D/4F dilution, 1:400, with antigen retrieval in 80% formic acid for 20 min) (Abcam). Immunohistochemical stains for PBBSs were performed with the monoclonal antibody 8D7 directed against the C terminus of the molecule at the dilution of 1:200, after antigen unmasking in a microwave oven for 30 min in 1 mM ethylenediaminetetraacetic acid, pH 8. This antibody was supplied by Dr. Pierre Casellas. Immunohistochemical reactions for PBBS were performed in sections from the superior frontal gyrus, hippocampus, putamen and globus pallidus, cerebellar hemisphere, and midbrain.

RESULTS

^{11}C-(R)-PK11195 Images

The algorithm used for the extraction of the whole-blood tracer time course worked well with all the subjects considered in the study by selecting pixels that were adjacent in the same slice or in the same position in 2 contiguous slices in likely locations for venous sinuses. Figure 1 displays an example of the extracted $C_B(t)$ for 1 control. The average whole-blood concentration curves of controls and patients with AD were compared. Figure 2 shows the average $C_B(t)$ for the 10 controls and the 10 patients with AD, in which the curves were obtained averaging the curves of the controls and patients with AD, decay-correcting the 2 resulting time–activity curves, and then fitting to each of them, from the peak onward, a biexponential plus constant function. The figure displays only the values from 3 min on (from scan 6 onward) to better emphasize the result that can be easily visually assessed.

The blood-extraction algorithm showed a significant robustness with the number of pixels used for the computation

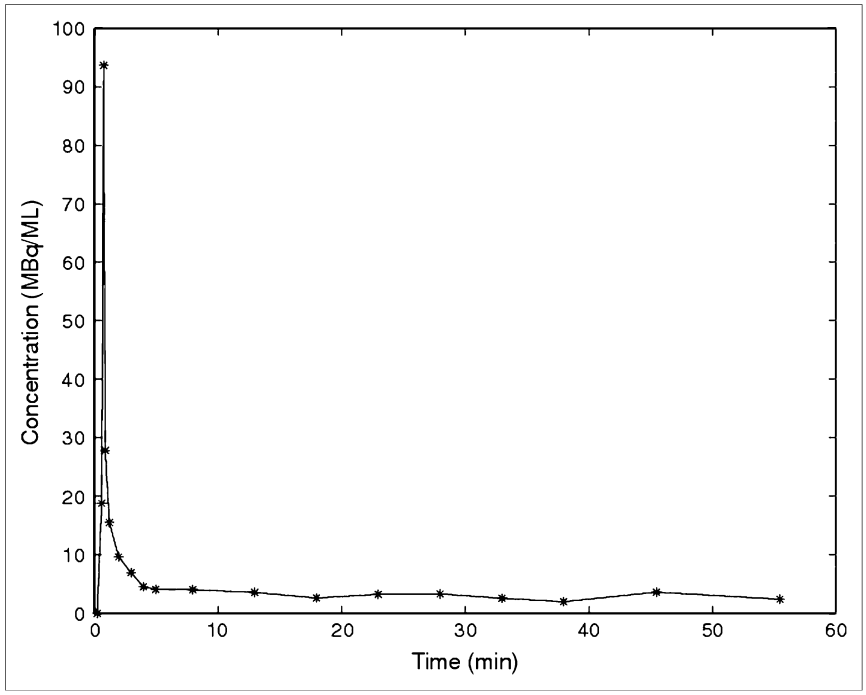

FIGURE 1. Example of extracted $C_B(t)$ for healthy control (*).

of the whole $C_B(t)$. A linear correlation between Vb estimated using 10 pixels for $C_B(t)$ and the corresponding Vb computed using 5 pixels yielded 0.955 as the slope and 0.003 as the intercept ($R^2 = 0.975$) (Fig. 3). Similar results were obtained when Vbs estimated using 20 pixels for $C_B(t)$ were compared with Vbs estimated using 10 pixels for $C_B(t)$, which will be the only Vb estimate considered for the rest of the analysis. Average Vb values obtained for controls were higher than those obtained for patients with AD for all ROIs considered, as displayed in Figure 4, which shows the mean Vb for each ROI for controls compared with the corresponding mean Vb for the AD group ($Vb^R = 5\%$). The global mean of cerebral blood volume, averaged over all ROIs and subjects, was 4.22% for controls and 2.87% for patients with AD, with Vb^R fixed at 5%.

As previously explained, we tested the possibility of using fixed, albeit subject-dependent, values for Vb^R instead of fixing it to a common value. Because of the low signal-to-noise level of the data, this approach showed far less reliability than the previous one. Of the $11 \times 20 = 220$ total

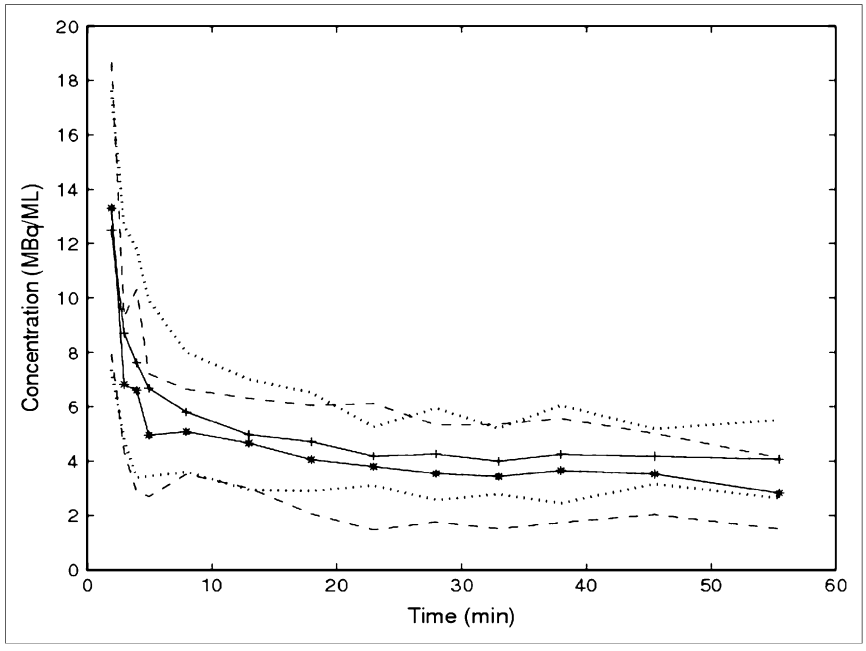

FIGURE 2. Average $C_B(t)$ for healthy controls (+) and patients with AD (*). Curves were decay-corrected and displayed from 3 min on (from scan 6) to better visually assess result. Dotted lines represent average $C_B(t) \pm$ SD for controls; dashed lines are average $C_B(t) \pm$ SD for AD.

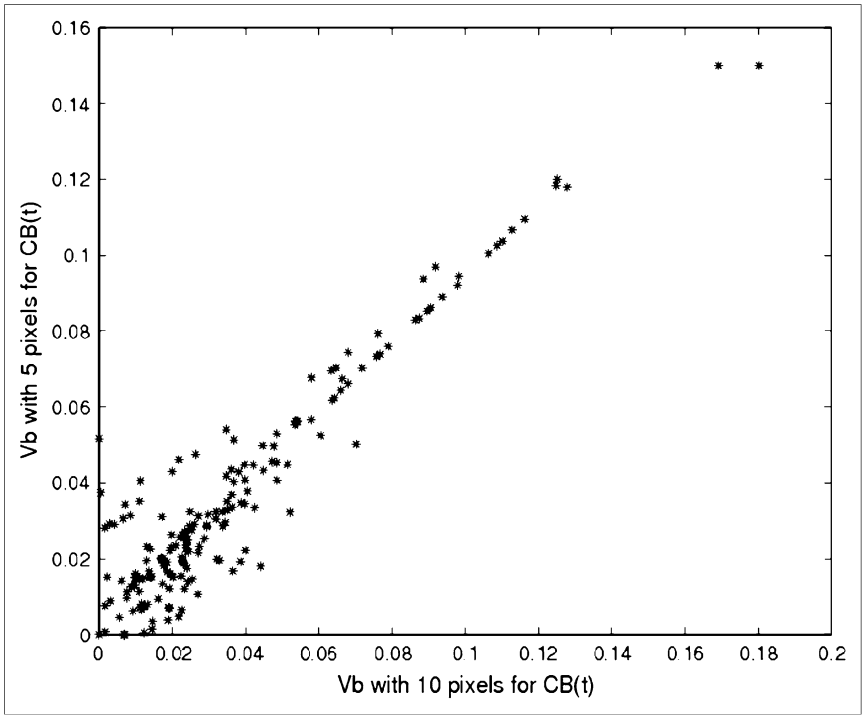

FIGURE 3. Estimates of blood volume (Vb) computed using 10 pixels for extraction of $C_B(t)$ (*x*-axis) plotted vs. corresponding Vb fraction estimates computed using 5 pixels (*y*-axis).

ROIs examined, roughly one half of Vb^R estimates reached either the maximum allowed value (10%) or the minimum allowed value (0%). Results of this approach are, therefore, not presented.

When Vb^R was changed from the standard value of 5%, the global mean of cerebral blood volume became 5.41%, 6.27%, and 7.14% for controls and 3.55%, 4.43%, and 5.4% for patients with AD with Vb^R fixed at 6%, 7%, and

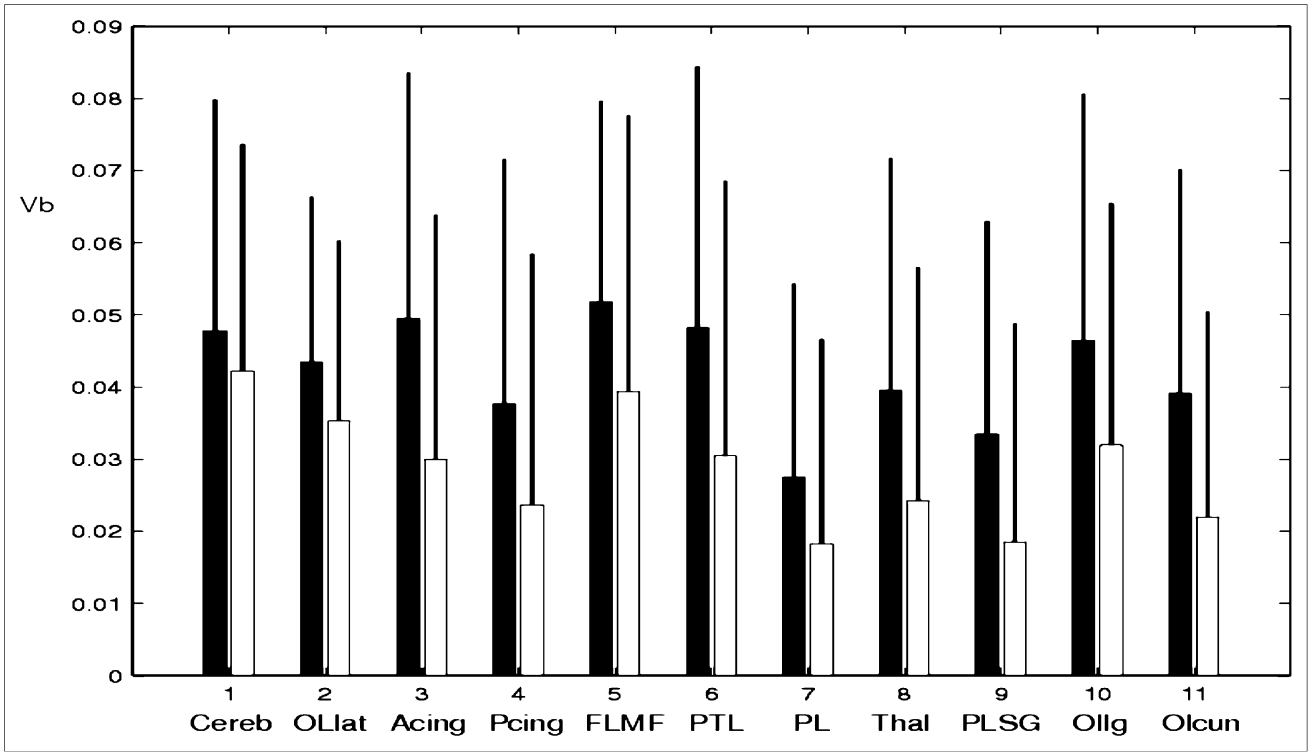

FIGURE 4. Average blood-volume (Vb) component estimates for controls (black bars) and patients with AD (white bars) with Vb^R set to 5% for each of 11 considered ROIs. ROIs were cerebellum (cereb), lateral occipital lobe (OLlat), anterior cingulate gyrus (Acing), posterior cingulate gyrus (Pcing), frontal lobe middle frontal gyrus (FLMF), posterior temporal lobe (PTL), parietal lobe (PL), thalamus (Thal), superior parietal gyrus (PLSG), occipital lobe lingual gyrus (Ollg), and occipital lobe cuneus (Olcun).

8%, respectively. Therefore, an evident monotonous positive dependence of estimated target Vb on Vb^R was demonstrated. For all 11 ROIs and all 4 values of Vb^R (0.05, 0.06, 0.07, and 0.08), however, the mean of the AD Vb was always lower than the corresponding mean of the control Vb. Also, BPs increased with increasing values of Vb^R; the means of BPs of healthy subjects were 0.683, 0.699, 0.713, and 0.734 for a Vb^R of 5%, 6%, 7%, and 8%, respectively. This increase was, however, very slight, and correlation between BP (5%) and the other 3 sets of BPs (6%, 7%, and 8%) was excellent (R^2 = 0.999, 0.991, and 0.989, respectively). Because assuming different Vb^R fixed values does not change the trend of the AD versus control results, all the following results refer to the case of Vb^R = 5%.

The BP estimates obtained with the SRTMV correlated with BPs obtained with the SRTM (R^2 = 0.97). Figure 5 displays the BP estimates for both controls and patients with AD. The slight overestimation of BPs of SRTMV with BPs of

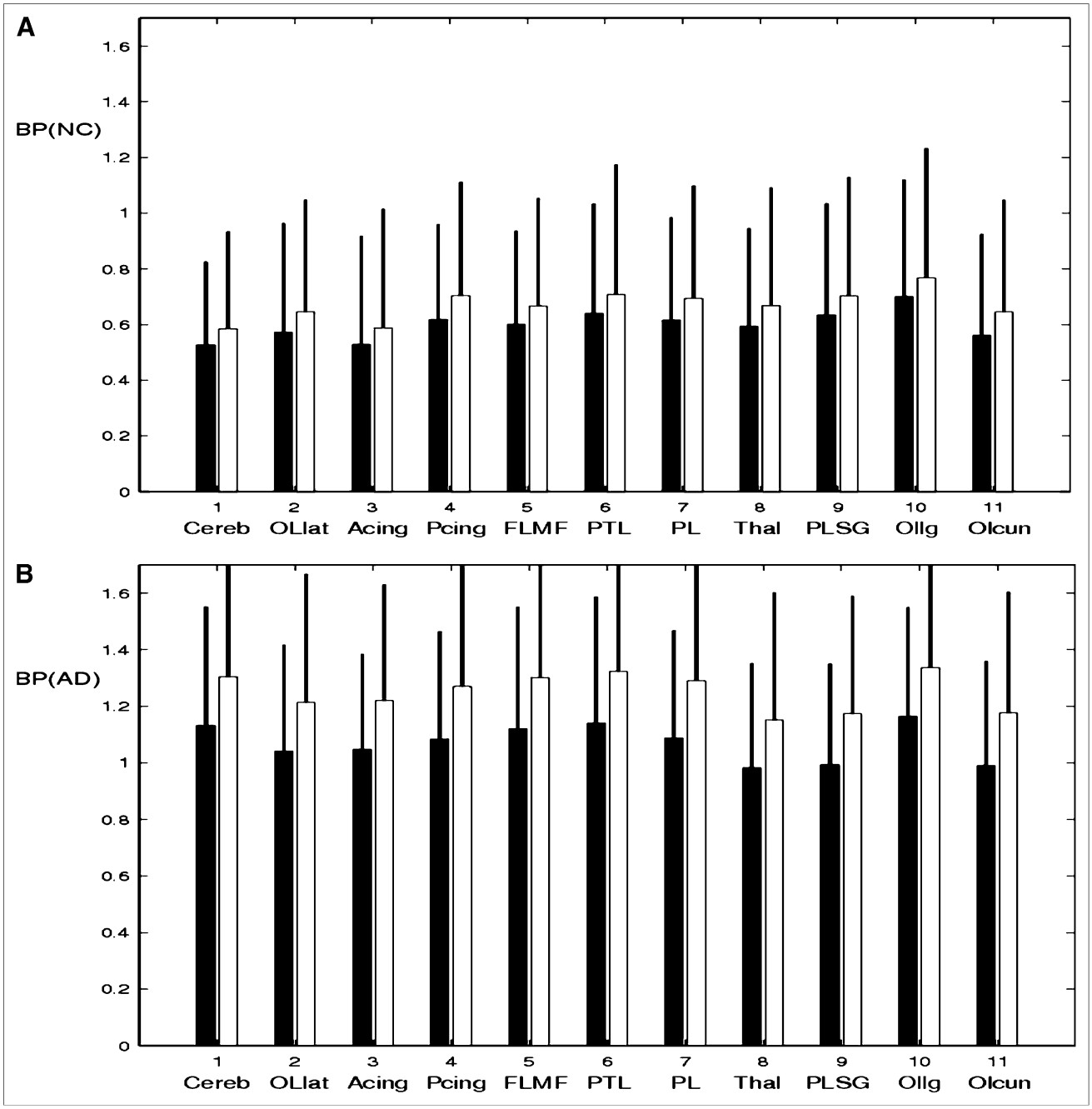

FIGURE 5. Average BP for controls (A) and patients with AD (B). In each image, SRTM and SRTMV values are displayed as black bars and white bars, respectively. ROIs were cerebellum (cereb), lateral occipital lobe (OLlat), anterior cingulate gyrus (Acing), posterior cingulate gyrus (Pcing), frontal lobe middle frontal gyrus (FLMF), posterior temporal lobe (PTL), parietal lobe (PL), thalamus (Thal), superior parietal gyrus (PLSG), occipital lobe lingual gyrus (Ollg), and occipital lobe cuneus (Olcun).

SRTM correlates with what was found by Bertoldo et al. (*13*). The BPs of AD, however, increased more than BPs of controls (global average increment of 0.07 for controls and of 0.18 for AD, corresponding to increments of 11.9% and 16.8%, respectively) (Fig. 5). This fact brought about a decrease of *P* values in the 1-tailed *t* test comparing BPs of controls with BPs of AD. For the 11 ROIs, *P* values decreased 33% on average, from 0.0008, 0.0068, 0.0025, 0.0049, 0.0038, 0.0082, 0.0056, 0.0131, 0.023, 0.096, and 0.0085 to 0.0007, 0.0042, 0.0017, 0.0049, 0.0030, 0.0062, 0.0029, 0.0118, 0.0112, 0.0077, and 0.0052.

Pathologic Examination

The brains of the 3 young subjects showed no evidence of arteriosclerotic changes. Small- and medium-size intraparenchymal arteries and leptomeningeal arteries demonstrated strong PBBS expression in endothelial cells and in smooth muscle cells of the tunica media (Fig. 6A). In contrast, we observed a decrease in PBBS expression in vessels of brains of elderly subjects (Fig. 6B) and a marked loss of expression in all 3 cases of patients with AD (Figs. 6C and 6D). Lack of PBBS staining in both elderly controls and patients with AD was mainly because of fibrosis of the tunica media and, to a lesser extent, because of damage of the endothelium.

DISCUSSION

The extensive use of ^{11}C-(*R*)-PK11195 and PET to monitor microglial activity in the central nervous system stems from the high specificity of microglial activity for PBBS, a protein consistently upregulated in microglial cells when reacting to any insult to brain tissue. However, the concomitant expression of PBBS in the vasculature prompted this investigation into the effect of the vascular-specific component into the quantification of microglia BPs.

Brain vessels possess peculiar anatomic and physiologic properties because of their role in the exchange processes of various substances between the blood and brain, which are highly regulated for the maintenance of the neuronal environment. Age-related and amyloid-induced pathologic changes of the cerebral microvasculature have been implicated as potential contributing factors to the pathogenesis of AD, possibly leading to neurofibrillary degeneration, plaque formation, and cell loss (*9*). Hence we chose AD as the experimental model to test the introduction of a blood component into reference and target regions using a modified version of SRTM called SRTMV.

By applying our SRTMV, we observed a decrease of the estimated vascular tracer activity fraction in patients with AD, compared with controls, and an increase of BPs that was significantly greater for AD than for controls. These results are consistent with what was found by Bertoldo et al. (*13*).

These findings can be interpreted as a consequence of the significant changes of the vascular structure in AD, which have been described previously (Farkas and Luiten (*17*) provided a comprehensive review). In AD, a thickening of the basement membrane that surrounds endothelial cells is frequently observed (*18*), together with the degeneration of

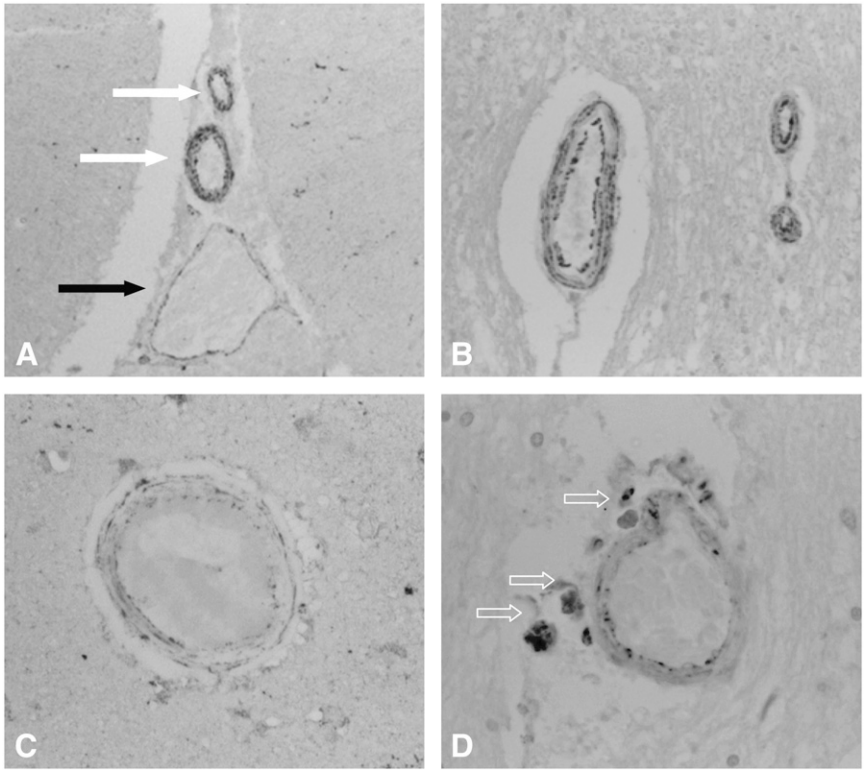

FIGURE 6. Expression of PBBS in healthy (NC) and AD brains visualized by immunocytochemistry. (A) Young control: slide shows strong expression of protein in leptomeningeal arteries (white arrows) and low expression in veins (black arrow). (B) Elderly control: lower PBBS expression in medium- and small-size arteries with moderate fibrosis. (C) Patient with AD: expression is almost entirely absent in severely fibrotic artery in frontal cortex. (D) Patient with AD: PBBS labeling is reduced in fibrotic artery in frontal cortex, but protein is upregulated in surrounding macrophages (arrows).

smooth muscle cells that are responsible for vascular contractility (*19*). Both conditions determine a narrowing of the lumen, therefore causing a decrease in blood volume that is then reflected in the reduced vascular fraction term Vb. At the same time, immunohystochemistry confirmed a remarkable loss of PBBS in the vasculature in endothelium and smooth muscles in patients with AD and, to a minor extent, in elderly subjects, compared with healthy young subjects. This would also be reflected in Vb. Therefore, the compounded effect of lumen reduction and reduced PBBS vascular density would then reflect in a smaller Vb and a greater volume of distribution for the target region, with the resulting greater increase of BPs in patients with AD than in controls.

The introduction in the SRTMV of the vascular term Vb seems to have captured both phenomena effectively and confirmed that application of simple SRTM in ^{11}C-(*R*)-PK11195 studies of patients with AD, compared with matched controls, may lead to an underestimation of microglial activity.

The use of a fixed value of 5% for Vb^R for all subjects may be questionable; Vbs are on average smaller in AD, and it seems appropriate to assume that Vb^R also decreases in AD. We decided to use the same value because the reference time course, despite being subject-dependent, should not, in theory, reflect the differences between healthy and ill conditions.

For the quantification of Vb, the modification of SRTM to account for blood volume was originally proposed by Gunn et al. (*12*) and subsequently developed and applied by Bertoldo et al. (*13*). In addition to being totally noninvasive, SRTMV yielded BP estimates that were systematically slightly higher but in excellent correlation with SRTM BP estimates and could, therefore, be used as a substitute for conventional SRTM when vascular signal plays an important role.

The procedure used for the extraction of the blood component from images is less sophisticated than others that are available for the accurate estimation of the blood tracer concentration–time course. The procedures use cluster analysis reported by Liptrot et al. (*20*), accurate definition of the vascular region with appropriate correction for spillover and partial volume demonstrated by van der Weerdt et al. (*21*), or resolution of nonlinear problems to determine the arterial concentration for each subject reported by Wang et al. (*22*). However, these procedures often require 1 or more blood samples, making them slightly invasive, and as the estimated arterial input function is used as the forcing function of the system, its estimate must be absolutely reliable. In SRTMV, the forcing function is the concentration in reference tissue over time, and BP estimates are less dependent on $C_B(t)$. Hence, in our context a reliable approximation of only the whole-blood tracer concentration was necessary, and the simple yet effective algorithm described was selected because of its computational speed and simplicity. Moreover, this approach displayed a significant robustness with the number of pixels used for the $C_B(t)$ computation when Vb and BPs obtained with different $C_B(t)$ were compared.

CONCLUSION

The reduction of Vb^T in AD can be interpreted as a consequence of 2 independent but concurring phenomena. The vascular fibrosis in the AD brain causes the well-documented decrease of the size of lumens and the reduction of blood volume. At the same time, the fibrotic process determines the loss of vascular PBBS, particularly in smooth muscles, as here documented by immunochemistry. The inclusion of the additional vascular component in the SRTM effectively models these 2 concurrent processes and amplifies the BP in AD more than in controls because of the decrease in tracer binding to the vasculature in the disease cohort.

REFERENCES

1. Gebicke-Haerter PJ. Microarrays and expression profiling in microglia research and in inflammatory brain disorders. *J Neurosci Res.* 2005;81:327–341.
2. Banati RB. Visualising microglial activation in vivo. *Glia.* 2002;40:206–217.
3. Hertz L. Binding characteristics of the receptor and coupling to transport proteins. In: Giessen-Crouse E, ed. *Peripheral Benzodiazepine Receptors.* London, U.K.: Academic Press; 1993:27–51.
4. Turkheimer FE, Edison P, Pavese N, et al. Reference and target region modeling of [^{11}C]-(*R*)-PK11195 brain studies. *J Nucl Med.* 2007;48:158–167.
5. Kropholler MA, Boellaard R, Schuitemaker A, et al. Evaluation of reference tissue models for the analysis of [^{11}C](*R*)-PK11195 studies. *J Cereb Blood Flow Metab.* 2006;26:1431–1441.
6. Anderson AN, Pavese N, Edison P, et al. A systematic comparison of kinetic modelling methods generating parametric maps for [^{11}C]-(R)-PK11195. *Neuroimage.* 2007; 36:28–37.
7. Woolsey TA, Rovainen CM, Cox SB, et al. Neuronal units linked to microvascular modules in cerebral cortex: response elements for imaging the brain. *Cereb Cortex.* 1996;6:647–660.
8. del Zoppo GJ, Mabuchi T. Cerebral microvessel responses to focal ischemia. *J Cereb Blood Flow Metab.* 2003;23:879–894.
9. Iadecola C. Neurovascular regulation in the normal brain and in Alzheimer's disease. *Nat Rev Neurosci.* 2004;5:347–360.
10. Spinks TJ, Jones T, Bloomfield PM, et al. Physical characteristics of the ECAT EXACT3D positron tomograph. *Phys Med Biol.* 2000;45:2601–2618.
11. Hammers A, Allom R, Koepp MJ, et al. Three-dimensional maximum probability atlas of the human brain, with particular reference to the temporal lobe. *Hum Brain Mapp.* 2003;19:224–247.
12. Gunn RN, Sargent PA, Bench CJ, et al. Tracer kinetic modeling of the 5-HT1A receptor ligand [carbonyl-^{11}C]WAY-100635 for PET. *Neuroimage.* 1998;8:426–440.
13. Bertoldo A, Pietra L, Moresco RM, et al. Quantitative in vivo imaging of microglia activation using [^{11}C]PK11195 and two reference tissue models. *Neuroimage.* 2006;31(suppl 2):T79.
14. Cobelli C, Foster D, Toffolo G. *Tracer Kinetics in Biomedical Research: From Data to Model.* New York, NY: Kluwer Academic/Plenum; 2001.
15. Kropholler MA, Boellaard R, Schuitemaker A, et al. Development of a tracer kinetic plasma input model for (R)-[^{11}C]PK11195 brain studies. *J Cereb Blood Flow Metab.* 2005;25:842–851.
16. Gunn RN, Lammertsma AA, Hume SP, Cunningham VJ. Parametric imaging of ligand-receptor binding in PET using a simplified reference region model. *Neuroimage.* 1997;6:279–287.
17. Farkas E, Luiten PG. Cerebral microvascular pathology in aging and Alzheimer's disease. *Prog Neurobiol.* 2001;64:575–611.
18. Perlmutter LS, Chui HC. Microangiopathy, the vascular basement membrane and Alzheimer's disease: a review. *Brain Res Bull.* 1990;24:677–686.
19. Miyakawa T, Uehara Y, Desaki J, Kimura T, Kuramoto R. Morphological changes of microvessels in the brain with Alzheimer's disease. *Jpn J Psychiatry Neurol.* 1988;42:819–824.
20. Liptrot M, Adams KH, Martiny L, et al. Cluster analysis in kinetic modelling of the brain: a noninvasive alternative to arterial sampling. *Neuroimage.* 2004;21:483–493.
21. van der Weerdt AP, Klein LJ, Boellaard R, Visser CA, Visser FC, Lammertsma AA. Image-derived input functions for determination of MRGlu in cardiac ^{18}F-FDG PET scans. *J Nucl Med.* 2001;42:1622–1629.
22. Wong KP, Feng D, Meikle SR, Fulham MJ. Simultaneous estimation of physiological parameters and the input function: in vivo PET data. *IEEE Trans Inf Technol Biomed.* 2001;5:67–76.